Peer-reviewed version available at *Catalysts* **2019**, *9*, 328; doi:10.3390/catal9040328

Article

Synthesis and Characterization of Te Nanotubes Decorated with Pt Nanoparticles for fuel cell anode/cathode working at neutral pH.

Maria Rachele Guascito [1,*], Daniela Chirizzi [2], Emanuela Filippo [3], Francesco Milano [4], Antonio Tepore [3]

[1] Dipartimento di Scienze e Tecnologie Biologiche e Ambientali, Università del Salento, S.P. Lecce-Monteroni, 73100 Lecce, Italy; maria.rachele.guascito@unisalento.it
[2] IZS Puglia e Basilicata, U.O. Putignano. Via Chiancolla 1, C.da. S. Pietro Piturno, 70017 Putignano (BA), Italy; mailto:daniela.chirizzi@izspb.it
[3] Dipartimento di Beni Culturali, Università del Salento, S.P. Lecce-Monteroni, 73100 Lecce; antonio.tepore@unisalento.it (A. T.), filippo.emanuela@libero.it (E. F.)
[4] Istituto di Scienze delle produzioni Alimentari, Consiglio Nazionale delle Ricerche, S.P. Lecce-Monteroni, 73100 Lecce; francesco.milano@cnr.it
* Correspondence: maria.rachele.guascito@unisalento.it (M. R. G.)

Abstract: In fuel-cell technological development, one of the most important objectives is to minimize the amount of Pt, the most employed material as oxygen reduction and methanol oxidation electro-catalyst. In this paper we report the synthesis and characterization of Te nanotubes (TeNTs) decorated with Pt nanoparticles, readily prepared from stirred aqueous solutions of $PtCl_2$ containing a suspension of TeNTs and ethanol acting as a reducing agent, avoiding the use of any hydrophobic surfactants as capping stabilizing substance. The as obtained TeNTs decorated with Pt nanoparticles **(TeNTs/PtNPs**) have been fully characterized by X-ray diffraction (XRD), transmission electron microscopy (TEM), selected area diffraction patterns (SAD), X-ray photoelectron spectroscopy (XPS) and cyclic voltammetry (CV). We demonstrate that the new material can be successfully employed in fuel cell either as anodic (for methanol oxidation reaction) and cathodic (for oxygen reduction reaction) electrode with high efficiency in terms of related mass activities and on-set improvement. Remarkably, the cell operates in aqueous electrolyte buffered at pH 7.0, thus avoiding acidic or alkaline conditions that may lead e. g. to Pt dissolution (at low pH) and paving the way for the development of biocompatible devices and on chip fuel cells.

Keywords: Te nanotubes decorated with Pt nanoparticles; fuel cell neutral pH; oxygen reduction reaction; methanol oxidation reaction; X-ray photoelectron spectroscopy.

1. Introduction

Nanomaterials have become of paramount importance as advanced systems in numerous fields of research and technological applications mainly thanks to the high opportunity to finely tune the properties of the material by changing their dimensions.[1] In addition, nanomaterials with anisotropic shapes are characterized by higher surface area and several contact points (borders, inner and/or outer surfaces) that can be functionalized in numerous ways [2] if compared to the isotropic counterpart. In this context, carbon nanotubes and nanowires represented a breakthrough in the nano-science research in developing 1D anisotropic nanoparticles since their discovery in 1991.[3]

In electrocatalytic applications, the selection of the optimal electrode materials, to make anodes/cathodes suitable to develop advanced fuel cells and/or electrochemical detectors, is influenced for the most part by their surface chemical composition and physical properties, because the electro-oxidation/reduction rate of the electroactive substances severely depends from these parameters. In the last three decades, to enhance the electrochemical processes in these devices, there was an increasing interest to develop new innovative anisotropic nanomaterials in different shapes

and sizes to make chemically modified electrodes (CMEs), based on metal and/or multi-metallic nanostructures, thanks to their extraordinary electrocatalytic activity decreasing the over-potentials of many substances with respect to common unmodified electrodes [4]. Accordingly, almost since 1980, a variety of techniques and treatments have been developed, useful to modify the surface of the classical electrodes to obtain specific electrocatalytic properties by using either mono- or multi-metallic nanostructures. [5] Multi-metallic structures, either in form of alloy or nano-sized core-shell, show special characteristics like superior optical, catalytic, electronic, and magnetic properties, directly dependent from their chemical composition, as well as their nanometric dimensions typically superior to their pure element counterparts. [6] However, even if most of studies on the synthesis of alloy or core–shell nanostructures have been particularly devoted to develop isotropic spherical structures, methods for making alloy or core–shell structures with different anisotropic shapes, like nanowires, nanotubes etc., have also been reported. [7-9]

In this context platinum material has been extensively investigated and studied for its potentiality in technological applications, including catalysis in many chemical reactions and as electrode material, in fuel cells and/or electrochemical sensors development. On the other hand, massive application of expensive Pt-based catalyst implies a substantial increase in actual costs in fuel cells and/or sensors technologic development, thereby reducing their commercial competitiveness. To reduce the effective device cost by improving the electrocatalytic efficiency of electrode materials with the increment of the active surface, the use of platinum nanostructures in different suitable shapes (i.e. nanowires, nanotubes, nanoparticles) has been studied. [10-15] Besides, the presence of a different metal (e.g., Cu, Sn, Co, Ni, Pd, Au, Ag, Fe, Zn, Ru) to form platinum based hetero-nanostructures or alloy catalysts, can further reduce the Pt amount to be used, since these alloys exhibit better electrocatalytic properties than platinum monometallic counterpart nanomaterials. [16] This strategy is particularly helpful when Pt is used in combination with other inexpensive metals. Accordingly, works have been focused to synthesize and characterize new nanostructured materials based on Pt in different shapes like nanowires and nanoparticles, and, more recently, hollow structured nanomaterials (i.e. nanotubes, nanocages, hollow nanospheres) to make bimetallic and/or multi-metallic nanostructures, [6,17] operating in most cases in acidic or alkaline environment. However, considering that in acidic environment Pt can be dissolved, negatively affecting fuel cell and electrochemical sensor related performance, the use of neutral pH is desirable as it makes this detrimental effect less favorable. [18] In addition, in carbonaceous abiotic membrane-free fuel cells, the employ of electrolytic solution at pH 7.0 (near the buffering point of bicarbonate/CO_2) has been recently reported as a valid alternative to alkaline conditions in which the adsorption of CO_2, produced by carbonaceous electro-oxidation in the electrolyte, results in a pH decrease that induces instability in the performances of the alkaline direct methanol fuel cell (DMFC). [19,20] Finally, metal alloy materials (i.e. platinum based) used either as anode and cathode in fuel cell systems working at neutral pH can be applied in the development of advanced devices such as (bio-)fuel, micro-fuel and on-chip fuel cells. [20-23]

Pt electrodes modified with Te micro- and nanostructures have been proven to have higher activity than pure Pt bulk for ethanol and glucose electro-oxidation, and H_2O_2 electro-reduction, making them an important material for the improvement of carbonaceous fuel cells (i.e. direct alcohol fuel cells, DAFCs) [24] and as enzyme-less glucose and H_2O_2 sensors, [25,26] able to operate with high efficiency also under safe neutral pH environment.

In this work we report a study on the synthesis and characterization of Te nanotubes decorated with Pt nanoparticles, having an equimolar Pt/Te ratio, readily prepared from aqueous solutions of $PtCl_2$ containing Te nanotubes (TeNTs) mixtures with ethanol present as a reducing agent in a stirred bath, without using any hydrophobic surfactant as capping and stabilizing agent. We demonstrate that the fully characterized new material is suitable to be efficiently used in direct fuel cell devices either as anodic and cathodic material working in neutral pH conditions to develop safe and bio-compatible devices for both oxygen reduction reaction (ORR) and methanol oxidation reaction (MOR) kinetically competitive with respect to acidic or alkaline electrolytic unsafe conditions.

Peer-reviewed version available at Catalysts 2019, 9, 328; doi:10.3390/catal9040328

2. Results

The Te nanotubes used in this work were straightforwardly prepared exploiting their natural tendency to form this kind of structure when the Te powder is heated at 400 °C under Ar atmosphere: at this temperature the Te atoms evaporate and condense forming nanotubes.[27] Scanning electron microscope images and X-ray diffraction patterns showed that the as-synthesized Te had a nanotubular single-crystalline morphology with a hexagonal cross-section. Te nanotubes were typically 0.5-6 mm in length and 150-450 nm in external diameter. For the nanotube decoration with Pt nanoparticles, an ethanolic suspension of these TeNTs was subsequently mixed with an aqueous solution of $PtCl_2$. By heating the solution, the reduction of Pt on behalf of ethanol is promoted and the formed Pt(0) deposits on the TeNT surface as nanoclusters. The relative amounts of TeNT and $PtCl_2$, temperature and reaction time were optimized in order to obtain structures containing equimolar fractions of Pt and Te. The TeNTs/PtNPs nanostructures were used to modify the GC electrode by simply drop casting an ethanolic suspension of decorated nanotubes onto the electrode surface. After solvent evaporation, the nanostructured film was stabilized by various cyclic voltammetry cycles until a steady state current was obtained and activated in H_2SO_4 0.5 M as usual for Pt electrodes. The modified GC electrodes were finally used for electrocatalytic methanol oxidation and O_2 reduction experiments, respectively.

2.1 Morphological and spectroscopic characterization.

The X-ray diffraction (XRD) pattern of **TeNTs/PtNPs** composite samples in Figure 1 shows that the stronger and sharpener peaks can be indexed according to the hexagonal crystal structure of tellurium [JCPDS No 36-1452] with lattice constant of a= 0.44579 nm and c= 0.59270 nm. Besides the reflection peaks corresponding to Te, a number of lines were found to coincide with the (111) (200) and (220) planes of the face-centered cubic (fcc) platinum structure, with lattice constant a=0.39231 nm [JCPDS no. 04-0802]. These observations suggested that both Te and Pt were well crystallized nanostructures.

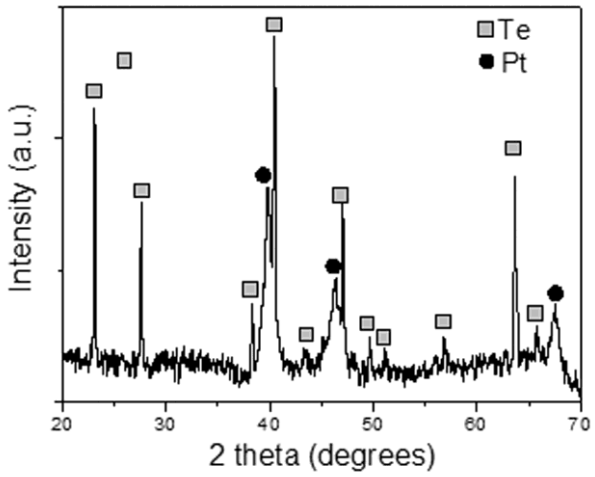

Figure 1. XRD pattern of TeNTs/PtNPs composite nanostructures

Figure 2b shows a representative transmission electron microscopy (TEM) image of straight tellurium nanotubes decorated with Pt nanoparticles. The nanotubes exhibited a tubular morphology with open prongs at the end and a mean diameter in the range 150-450 nm. TEM observations revealed also the presence of abundant nanoparticles, decorating the external surface of the nanotubes and with a diameter in the range 50-200 nm. The selected area diffraction pattern acquired on the extreme tip of the nanotube (Figure 2a) evidenced that the tubes grew along the [001] direction, in agreement with the preferred growth direction observed in our previous work.[27] The selected area diffraction pattern recorded on the nanoparticles assembly shown in Figure 2c, clearly exhibited diffraction rings with d spacing that could be indexed according to the fcc structure of Pt. In fact, the

Preprints (www.preprints.org) | NOT PEER-REVIEWED | Posted: 7 March 2019 doi:10.20944/preprints201903.0097.v1

Peer-reviewed version available at Catalysts 2019, 9, 328; doi:10.3390/catal9040328

concentric rings could be assigned as diffraction from {111}, {200}, {220}, {311} and {222} planes starting from the centermost ring.

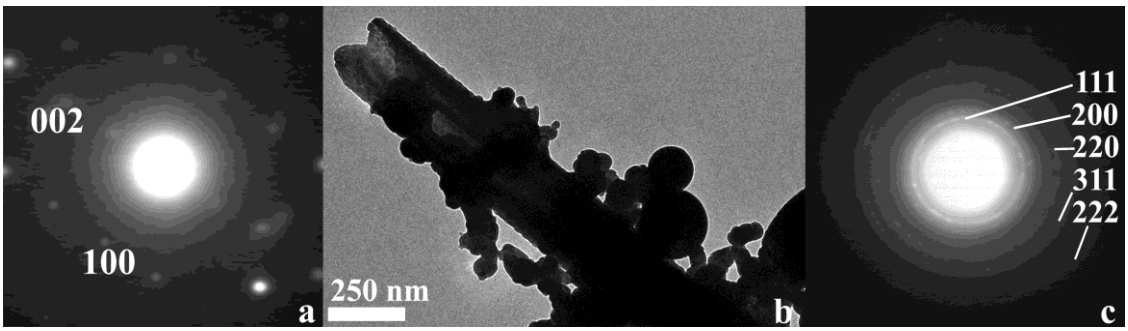

Figure 2. Typical TEM image of TeNTs/PtNPs composite nanostructures (b) along with selected area diffraction pattern recorded from the extreme tip of the nanotube (a) and nanoparticles assembly (c).

These results confirmed that the synthesized products were composed of Te nanotubes decorated with Pt nanoparticles.

XPS analysis was carried out on **TeNTs/PtNPs** samples. As expected, survey spectra of **TeNTs/PtNPs** samples showed the most intense **Pt4f** and **Pt4d** photopeak signals from platinum top-layer nanoparticles, in addition to **O1s**, **C1s**, **Te3d**, **Te4d** and **Te** (**M4N45N45**) base signals. **C1s** peak signals were attributed to carbon-containing species present as structures contaminations, while **O** peak signals could be attributed both to carbonaceous contamination (O1s peak component at 532.5 ± 0.1eV, NIST), and Te/Pt oxidized species coming from the top layer of the samples (O1s peak component at 530.7 ± 0.1eV, NIST), data not shown. The high resolution (HR) regions of **Te3d** and **Pt5f** were employed to investigate the **TeNTs/PtNPs** surface chemical speciation and composition. Figure 3A shows the main peak pair **Te3d**$_{5/2}$ and **Te3d**$_{3/2}$. To fit **Te3d**$_{5/2}$ and **Te3d**$_{3/2}$ HR region, typically three peak pair components were employed. According to literature data, [28,29] the peak pair at lower BE (572.8 ± 0.1eV and 583.2± 0.1eV) was attributed to Te(0). Instead, while the peak pair component at higher BE (576.0 ± 0.1eV and 586.4± 0.1 eV) was associated to Te (IV) oxide of the surface (TeO_2), the peak pair at 574.1 ± 0.1eV and 584.5± 0.1 eV was attributed to Te-Pt interacting phase. [28] The calculated tellurium atomic relative percentage (At. %) was 65 % of Te(0), 25% of Te(IV) and 10% of Te-Pt. Typically three peak pair components were also used to fit **Pt4f**$_{7/2}$ and **Pt4f**$_{5/2}$ HR region (Figure 3B). The most intense peak pair was Pt(0) at 71.3± 0.1eV and 74.1 ± 0.1eV (NIST) (At. % 73), the second peak pair (72.3 ± 0.1eV and 75.7 ± 0.1eV) was Pt-Te interacting phase (i.e. platinum nucleation sites inter-phase) (At. % 23). The last peak pair at 73.2 ± 0.1eV and 76.9 ± 0.1eV, according with NIST data and measured $PtCl_2$ standard (**Pt4f**$_{7/2}$ 73.5 ± 0.1eV) was attributed to $PtCl_2$ present as traces and coming from the synthesis process considering also the concomitant presence of Cl2p peak signal in survey spectrum. XPS Pt/Te elemental ratio was estimated to be about 1.4 confirming the platinum surface enrichment of tellurium nanotubes according also with TEM results.

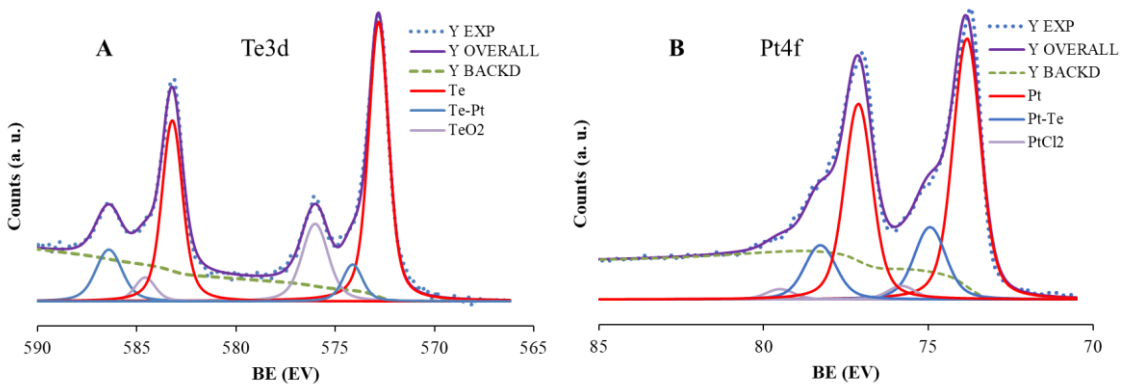

Figure 3. HR Te3d (A) and Pt4f XPS peaks related to TeNT/PtNP composite nanostructures.

In our experiments, outer surface of Te nanotubes served as substrate for the nucleation and growth of Pt nanoparticles. $PtCl_2$ was reduced by ethanol to form Pt nanoparticles, which will attach on the surface of Te nanotubes. It is reasonable to suppose that, likewise what happens in the case of the coating of selenium nanowires with Pt,[30] two distinct reduction reactions pattern occurred: an initial reduction of Pt(II) salt by Te template itself at the interface promoting the Pt nucleation process, in accord with the presence of characteristic Pt-Te interacting species (i.e. XPS experiments) and the reduction of the Pt(II) salt by the alcohol reagent that now promote the growth of the Pt nucleation sites. The galvanic reduction of the Pt(II) by Te template caused the formation of some nucleation sites for Pt nanoparticles formation, randomly distributed along the nanotubes and detected by XPS thanks to its high surface sensibility. As the reaction proceeded, Pt(II) salt reduction by alcohol became dominant, causing a gradual growth of the nanoparticles decorating the nanotubes and, at the same time, the formation of nanoparticles in the solution. The latter ones could attach to the outer surface of the Te nanotubes or to the Pt nanoparticles randomly formed on them.

2.2 Electrochemical characterization of TeNT/PtNP materials onto GC electrodes

Cyclic voltammetric experiments were used to study the main electrochemical properties of bimetallic composite **TeNTs/PtNPs** materials cast onto GC disk electrodes in phosphate buffer (pH 7.0) (Figure 4). In direct scan (oxidation) two peaks were observed respectively at +285 mV and at +520 mV attributed to Te(0)/Te(IV) and Pt(0)/Pt(II) processes associated also to the O_2 monolayer adsorption.[28,31] In reverse scan the peak observed in reduction at +100 mV is ascribed to Te(IV)/Te(0) and Pt(II)/Pt(0) overlapped peaks that involve species formed/adsorbed in oxidation scans. [28] This is in accord with the parallel increase of related currents, in oxidation and reduction, observed in the potential range between -100mV and +800 mV. The peak at -276 mV can be tentatively attributed to reduction processes of Te and Pt sites (i.e. different Te/Pt sites on anisotropic nanotube shapes) requiring higher overpotentials. However, since the overall currents increase with cycling, particularly in the region of Pt/Te reduction zone between -200 mV and +200 mV,[28] the potential scan probably restructures the Pt and Te atoms surface distribution due to the dissolution/re-deposition of different Te and Pt species as function of the voltammetric cycle numbers, accounting for the rising of the peak in reduction at +150 mV, a potential closer to the value of +50 mV already observed on Pt-Te similar bimetallic system and correlated principally to Pt species reduction.[28] The measured PtO_2 reduction peak in the same conditions on bare Pt is at +50 mV.[32] Moreover, a steady-state current, corresponding to a stable surface composition, is typically reached after about 30 CV cycles, necessary to obtain suitable **TeNTs/PtNPs/GC** modified electrodes.

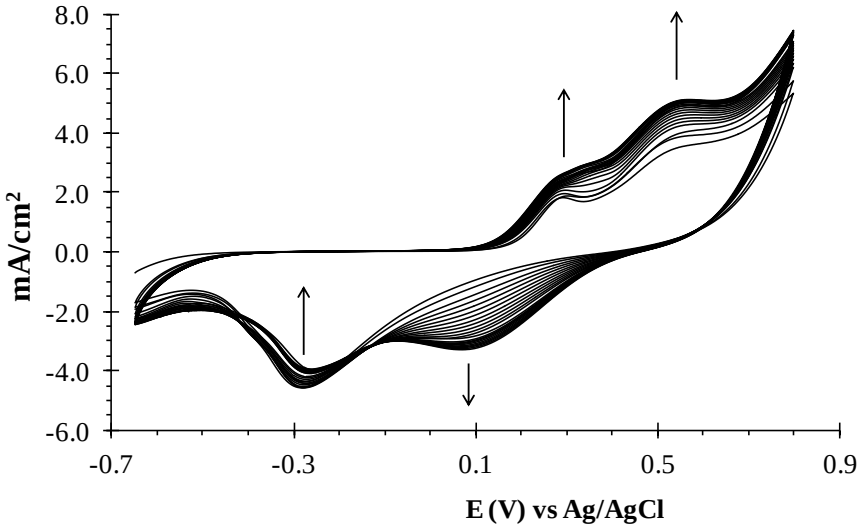

Figure 4. Characterization of TeNT/PtNP materials onto GC electrodes by cyclic voltammetry in phosphate buffer, pH 7.0. Scan rate 50 mV s^{-1}. Upward and downward arrows indicate the current change in the subsequent CV scans.

The as prepared **TeNTs/PtNPs/GC** electrodes were electrochemically activated in H_2SO_4 0.5 M before using in methanol electro-catalysis in neutral pH experiments, since preliminary tests suggested that a significant increase of the catalytic currents were reached after these pre-treatments. CV results reported in Figure 5 compare typical voltammograms recorded onto clean GC (curve a) and Pt (curve b) conventional electrodes as controls, and onto **TeNTs/PtNPs/GC** modified electrodes, in a clean phosphate buffer solution. All CV curves were obtained at scan rate of 50 mVs^{-1} in the potential range between -650 mV and +800 mV. As expected, conventional bare GC electrode do not show any specific electrochemical activity (Figure 5, curve a and related inset). Instead an evident electrochemical activity was recorded both on conventional bare Pt electrode (curve b) and **TeNTs/PtNPs/GC** modified electrode (curve c). Characteristic peaks due to the atomic hydrogen adsorption and desorption on platinum active sites were observed in the cathodic "hydrogen region" in neutral pH electrolytes, between -650 mV and -200 mV *vs* Ag/AgCl,[33,34] either on bare Pt and **TeNTs/PtNPs/GC** modified electrodes. So modifying the electrochemically inert GC electrode surface with **TeNTs/PtNPs** nanostructures, the electrochemical hydrogen adsorption/desorption processes can be activated as typically observed on bare platinum in the potential range between -520 mV and -220 mV at neutral pH, after activating it in H_2SO_4 0.5 M. In addition, besides the intense activity in "hydrogen region", **TeNTs/PtNPs/GC** modified electrodes showed in oxidation a well stable peak at E_{pa} = +500 mV with a peak in the reverse scan at E_{pc} = +150 mV attributed to both Pt(0)/Pt(II) and Te(0)/Te(IV) not well resolved red-ox processes related peaks. Otherwise, the shoulder at -140 mV has been attributed principally to Te(IV)/Te(0) reduction process.[26] In detail, charge amount (Q_H) exchanged during hydrogen desorption on **TeNTs/PtNPs/GC**, was almost 4 mC cm^{-2} in actual experimental conditions. Correspondent electrochemically active surface area (**ECSA**), that can provide important information relatively to the number of Pt sites catalytically active available for an electrochemical reaction,[32] was estimated to be 20 m^2/g_{Pt} by the following relation:[12]

$$\mathbf{ECSA = QH/(qH \times mPt)}$$

where $\mathbf{Q_H}$ is the charge amount exchanged during hydrogen desorption on Pt nano-particle sites in the "hydrogen region", $\mathbf{q_H}$ = 210 μC cm^{-2} is the charge required to oxidize a monolayer of H_2 on Pt surface and $\mathbf{m_{Pt}}$ = 7 μg is the amount of platinum loaded on the electrode. This value has been estimated by considering the amount of Pt/Te composite solution cast on the electrodes and corrected taking into account the efficiency of **TeNTs/PtNPs** deposition obtained by the $Q_{TeNT/PtNP(ox)}/Q_{TeNT/PtNP/GC(ox)}$ ratio estimated almost 3:1, where, $\mathbf{Q_{TeNT/PtNP(ox)}}$ has been obtained considering the overall charge quantities related to the platinum/tellurium oxidation measured in the steady-state condition (Figure 4, last cycle) and $\mathbf{Q_{TeNT/PtNP/GC(ox)}}$ the overall charge related to the platinum/tellurium oxidation of the same modified electrodes as obtained in phosphate buffer after their activation in H_2SO_4 0.5 M (Figure 5, curve c).

Preprints (www.preprints.org) | NOT PEER-REVIEWED | Posted: 7 March 2019 doi:10.20944/preprints201903.0097.v1

Peer-reviewed version available at Catalysts 2019, 9, 328; doi:10.3390/catal9040328

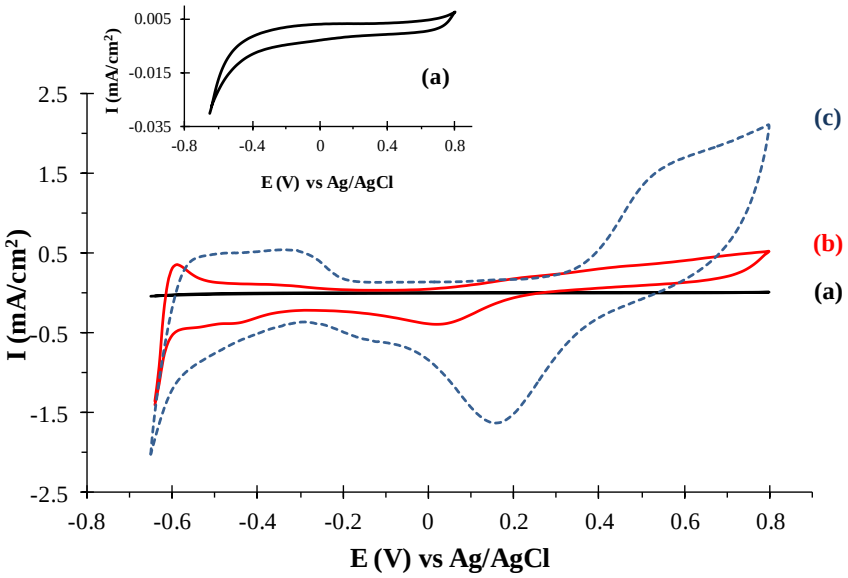

Figure 5. Characterization of GC (curve a), bare Pt (curve b) and TeNT/PtNP/GC (curve c) electrodes by Cyclic Voltammetry in phosphate buffer, pH 7.0. Scan rate 50 mV s^{-1}.

2.3 Electrochemical characterization of TeNT/PtNP/GC modified electrodes with respect to methanol oxidation.

The electrocatalytic activity of the as-obtained modified electrodes for the methanol oxidation reaction (MOR) was studied in phosphate buffer at pH 7.0, a neutral safe medium, by cyclic voltammetry at 100, 500 and 1000 mM methanol, respectively. Related voltammograms are shown in Figure 6 A, B and C (green traces) and compared to bare GC (red traces) and bare Pt (blue traces) electrodes as obtained and in Figure S1 after subtraction of the relative background. Conventional GC electrode, as expected, was totally inactive with respect to methanol oxidation with current densities level ranging between -30 and 10 μAcm^{-2}. Otherwise bare Pt electrodes present peaks in oxidation and reduction related to the electrochemical activity involving the different oxidation states of platinum showing a typical electrocatalytic activity toward methanol oxidation in the potential range between 0.00 mV and +600 mV and a maximum of current density at around +370 mV vs Ag/AgCl, according to the reported values at platinum electrodes in neutral pH *vs* small molecular weight alcohols.[35-37] However, a rapid poisoning of the electrode at these high concentrations of methanol is observed. As a matter of fact, CV curves obtained at 500 mM (figure 6 B, trace Blue) and 1000 mM (figure 6 C, trace Blue) are almost coincident, with a tendency to decrease with the increase of methanol concentration. A remarkable catalytic oxidation current density, ranging between 0.0 and 4.0 μAcm^{-2}, for methanol on the **TeNTs/PtNPs** catalyst modified GC is observed in a wider potential range from -200 mV to +800mV. A consistent decrement of the methanol oxidation potential on-set, estimated to be almost of 150 mV if compared to bare Pt, is observed. The onset potential of methanol oxidation is an important factor in electrocatalytic study because it represents the power to break the methanol C-H bonds and the effectiveness in removing off species partially oxidized adsorbed on the electrode surface, improving with onset potential lowering. This observed behaviour, together with the overall current density increment, and the potential range raising in forward scan, with respect to bare Pt, confirms a synergic interaction between Te and Pt electroactive sites that act to enhance methanol electro-oxidation processes.

Accordingly, the specific activities, measured at the corresponding higher peak potential in forward scan at three different methanol contents (100, 500, and 1000 mM) are 2.24 mA cm^{-2} (at +298 mV), 3.22 mA cm^{-2} (at +547 mV) and 4.04 mA cm^{-2} (at +615 mV) respectively. Related mass activities are 448 mA $mg_{(Pt)}^{-1}$, 644 mA $mg_{(Pt)}^{-1}$ and 1615 mA $mg_{(Pt)}^{-1}$, respectively (Figure 6 D). All these values are comparable and/or better than recent previous data reported for methanol electro-oxidation as obtained, for example, on highly dispersed platinum nanoparticles/carbon nitride materials in acid

media,[38] on branched Pd and Pd-based trimetallic nanocrystals (NCs) with long, thin branches and open structures operating in basic media,[39] as well as on Pt/Te bimetallic nanowires.[40] The oxidation peaks recorded in backward scan (at +160mV, +440mV, and +530 mV) were attributed to the removal of incompletely oxidized carbonaceous species formed in forward scan on Pt, Te and Pt-Te active sites, which appear to be heavily influenced on the three different concentrations of methanol tested. A similar behaviour, where different electrocatalytic sites are activated (see the different peaks involved in CV experiments, Figure 6), not observed on previous reported Pt/Te bimetallic and Pt/Pd/Te trimetallic systems in acid pH [40,41] could be attributed to the coexistence on the top of the surface of Te-Pt *ad-atoms* directly involved in methanol electrocatalytic oxidation. The observed synergy plays a central role in reducing the on-set, as well as the poisoning effect at potentials greater than +350 mV observed in methanol electro-oxidation on bare Pt. Accordingly, in the potential range between +350mV and +800 mV, peak currents at +547 mV and +615 mV rise with methanol concentration increment. Finally, consistently a high platinum catalytic activity to the TeNT/PtNP/GC electrodes is not only confirmed but further enhanced in the "hydrogen region" in methanol presence. The observed current density that ranges from -2.0 to 0.5 $mAcm^{-2}$, in phosphate buffer methanol -free (Figure 5), increases ranging between -3.0 to 1.0 $mAcm^{-2}$ in methanol 500 mM. A saturation effect has been observed at methanol 1000 mM (Figure 6).

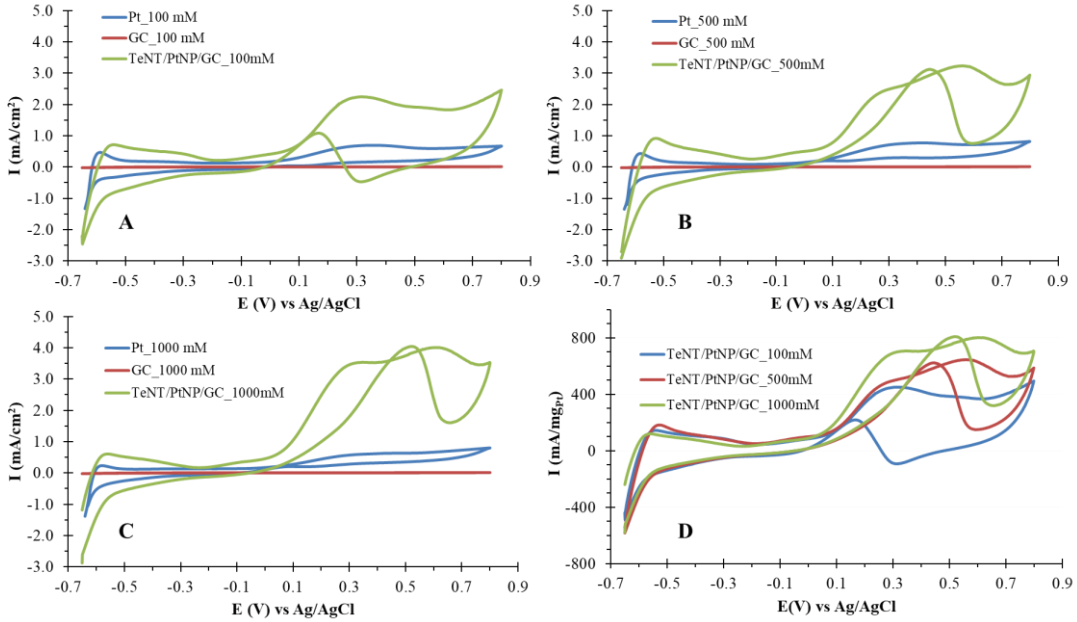

Figure 6. Cyclic voltammetric curves as obtained on bare GC (red traces), bare Pt (blue traces) and **TeNT/PtNP/GC** (green traces) electrodes, in phosphate buffer pH 7.0, respectively at 100mM (panel A), 500 mM (panel B) and 1000 mM (panel C) methanol solutions. Sweep rate 50 mV s^{-1}. The current density in panel D for **TeNT/PtNP/GC** electrodes is normalized in reference to the real Pt surface area per mass.

2.4 Electrochemical characterization of TeNT/PtNP/GC modified electrodes with respect to oxygen reduction.

The electrocatalytic activity of the **TeNT/PtNP/GC** toward the reduction of oxygen was studied in static conditions and compared to bare GC and Pt electrodes, at different O_2 content. Figure 7 A, B and C shows the typical CVs of oxygen electro-reduction at bare GC (red traces), bare Pt (blue traces), and **TeNT/PtNP/GC** modified GC (green traces) electrodes in phosphate buffer solution (pH 7.0) in N_2-saturated, in atmospheric O_2 and saturated O_2 conditions. All CVs were obtained at scan rate 50 mV s^{-1} in a potential range between -300 mV and +300 mV. Figure S2 shows the same CVs as obtained after subtraction of the relative background. As expected, GC electrodes (Figure 7 A, B, C; red traces) are totally inert. No catalytic reduction current density increment can be observed both in atmospheric O_2 and O_2-saturated solutions in the potential range employed, in comparison to N_2-saturated phosphate buffer. Otherwise, conventional Pt electrodes show a typical electrochemical activity rising in reduction with oxygen content increase (Figure 7A, B, C; blue traces), even if

Preprints (www.preprints.org) | NOT PEER-REVIEWED | Posted: 7 March 2019 doi:10.20944/preprints201903.0097.v1

Peer-reviewed version available at Catalysts 2019, 9, 328; doi:10.3390/catal9040328

moderate in comparison to **TeNTs/PtNPs/GC** modified electrodes. In fact, the higher current increment for oxygen reduction is observed on **TeNTs/PtNPs/GC** modified electrodes at both O_2 tested concentrations with respect to N_2-saturated solution (Figure 7 A, B, C green traces). In detail, on Pt electrodes the current density starts to increase at 0.00 mV reaching a quasi-plateau of -0.20 $mAcm^{-2}$ in atmospheric O_2 and at + 50 mV reaching a quasi-plateau of -0.30 $mAcm^{-2}$ in O_2-saturated solutions. Remarkably, **TeNTs/PtNPs/GC** shows larger density currents and peaks potentials in reduction between +50/+150 mV with on-set at +250 mV. These values are more positive than those measured on bare Pt characterized from a potential peak at -150 mV and on-set at +200 mV and quite similar to the recently reported value on Pt/C catalyst.[42] The more positive potential of the oxygen reduction peak indicates the higher ORR activity of the catalyst [42] demonstrating that the catalytic properties of Pt in **TeNTs/PtNPs/GCE** electrodes strongly depend on tellurium component. These data indicate that the current density rise observed on **TeNTs/PtNPs/GC** with O_2 concentration increment, and totally absent on GC, should be attributed to electrocatalytic oxygen reduction process on platinum nanoparticles, enhanced in presence of tellurium species. All these collected results point out that these hybrid nanostructures have excellent electrocatalytic activity for oxygen reduction in neutral pH, better than previous data obtained in similar static conditions on ultrathin platinum-coated gold nanoparticle monolayer films [43] as well as on tungsten nitride supported on carbon black [44] at acid pH, in agreement with the observation that Pt catalyst in neutral media promotes a mechanism involving direct $4e^-$ transfer [23]. Furthermore, the nanostructures show an electrocatalytic activity for oxygen reduction almost twice than the response obtained in neutral pH not only on Pt/C catalyst,[42] but also on Pt-free iron/polyindole-based electrocatalysts as recently reported.[42]

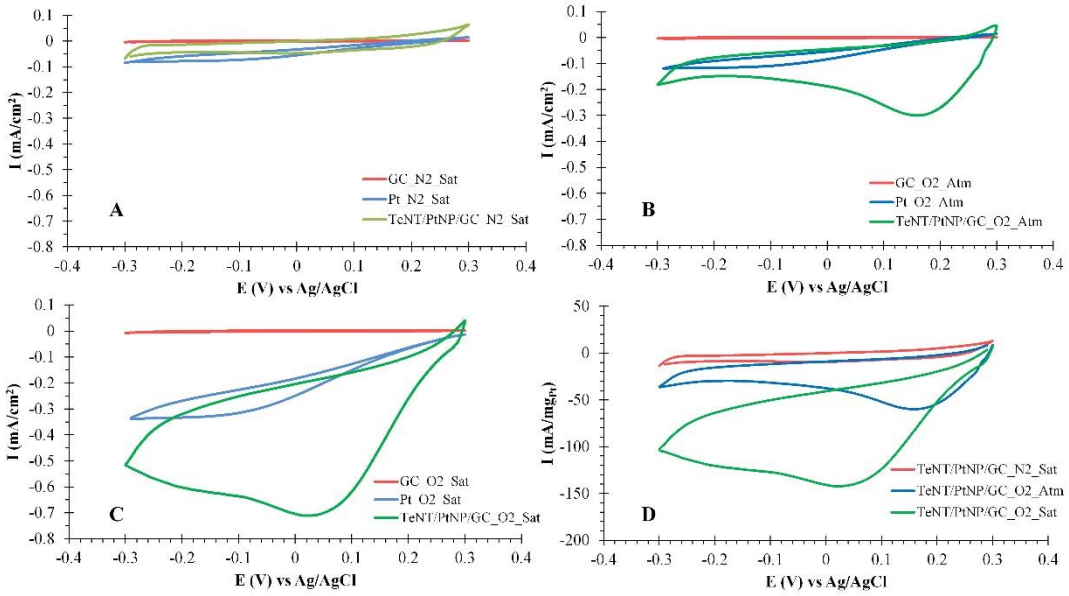

Figure 7. Cyclic voltammetric curves as obtained on bare GC (red traces), bare Pt (blue traces) and **TeNT/PtNP/GC** electrodes (green traces), in phosphate buffer pH 7.0, at N_2 saturated solution (panel A), O_2 atmospheric solution (panel B) and O_2 saturated solutions (panel C), respectively. Sweep rate 50 mV s^{-1}. The current density in panel D for **TeNT/PtNP/GC** electrodes is normalized in reference to the real Pt surface area per mass.

3. Materials and Methods

3.1 Chemicals

Tellurium powder (≥ 99.9%), $PtCl_2$, Na_2HPO_4, NaH_2PO_4, ethyl alcohol and methanol were analytical grade reagents furnished from Sigma and were used as received with no further

purification. Deionised ultra-filtered water prepared with a Milli-Q water purification system (Millipore Milli-Q, 18.2 MΩ cm^{-1}) has been used throughout the experiments.

3.2 Apparatus and Methods

All electrochemical experiments were carried out by using a μStat400 DropSens electrochemical potentiostat controlled by computer, in a conventional three-electrode cell by means of a glassy carbon (GC) (A=0.0707 cm^2) or Pt (A=0.0314 cm^2) disk working electrodes, a Pt wire as counter electrode and an Ag/AgCl, KCl (sat) as reference, in phosphate buffer solutions (pH 7.0, I = 0.2).

X-ray diffraction (XRD), transmission electron microscopy (TEM), selected area diffraction patterns (SAD) and X-ray photoelectron spectroscopy (XPS) were used to characterize the chemical structure and the morphology of the as obtained Te nanotubes decorated with Pt nanoparticles. X-ray diffraction measurements were obtained in the reflection mode on a Mini Flex Rigaku model diffractometer with Cu Kα radiation (λ = 0.154056 nm). The X-ray diffraction data were collected at a scanning rate of 0.02 degrees per second in 2 h ranging from 15° to 80°. The morphology and the crystal structure of the obtained nanostructures have been studied using a transmission electron Hitachi H-7100 microscope operating at an accelerating voltage of 100 kV. In order to prepare the Te nanotubes decorated with Pt nanoparticles samples for TEM observations, the samples were dispersed in ethanol; then, a little amount of this ethanol dispersion was dropped onto copper grids covered by carbon layer and let to dry slowly in air. XPS analysis was done by using the AXIS ULTRA DLD Kratos Analytical spectrometer. The Al Kα (1486.6 eV) monochromatic radiation source worked at 15 kV and 15 mA. In the analysis chamber the pressure was typically $3x10^{-9}$ torr. Widescan spectra and high resolution (HR) regions were registered in fixed analyzer transmission (FAT) mode. The pass energy (E_0) employed for survey regions acquisition was 160 eV with energy step of 1 eV, while in HR spectra acquisition, the pass energy was of 20 eV and energy step 0.1 eV. The hybrid lens mode was used for all measurements with analysis area of about 700 μm x 300 μm. During the analysis a neutralization charge system has been used. Data analysis and peak fitting were done by using the software New Googly [45] which allows background correction as well as curve-fitting of photoelectronic peaks. The peaks attribution, with an uncertainty on Binding Energies of ±0.1 eV, has been done by considering literature data and NIST reference database, [29] and referenced to the aliphatic carbon (C1s peak signal), as an internal standard, set at 285.0 eV [45].

3.3 Synthesis of tellurium nanotubes.

Large scale amounts of tellurium nanotubes were synthesized via a vapor deposition method as reported in a previous work and slightly modified. [27] Powder of tellurium was positioned in a quartz boat at the middle of a tube furnace and directly evaporated onto silicon slides as substrate (0.5x1.0 cm) located 20 cm apart, in a constant gas argon flow (100 sccm, 99.9%). In a typical experiment, the tube was rapidly heated in 20 min from room temperature to 400 °C under Ar flow and kept at this temperature for 40 min during which the Te evaporates and deposits on the silicon substrate spontaneously forming nanotubes. At that time the argon gas flow was stopped and the furnace cooled naturally to the room temperature. All silicon slides used as support for TeNTs deposition experiments were accurately washed by ultrasonication in a water and non-ionic detergent mixture, followed by thorough rinsing with water and ethanol to remove any remnants of nonionic detergent, and dried before use. Scanning electron microscope images and X-ray diffraction patterns showed that the as-synthesized Te had a nanotubular single-crystalline morphology with a hexagonal cross-section. The Te nanotubes were typically 0.5-6 mm in length and 150-450 nm in external diameter.

3.4 Synthesis of Te nanotubes decorated with Pt nanoparticles (TeNTs/PtNPs).

In a typical synthesis, Te nanotubes (30 mg) from previous experiments were dispersed in 20 mL of ethanol with vigorous magnetic stirring at room temperature. Then, platinum (II) chloride (10 mM) was added. The vial was capped and heated at 70 °C under magnetic stirring for 8 hours. The **TeNT/PtNP** nanostructures were washed several times in order to eliminate eventually not reacted

platinum chloride and chloride in excess. The elemental composition of synthesized TeNTs/PtNPs was estimated to be 50 % Pt and 50 % Te (At. %), in the hypothesis that all $PtCl_2$ was reacted.

3.5 Preparation of TeNTs/PtNPs/GC modified electrodes

Routinely, the CG electrode surfaces were polished with alumina, rinsed with deionized water and dried with N_2 flow. Modified electrodes were made by casting 5 μL of **TeNTs/PtNPs/ethanol** (8 mg/1 mL) suspension directly onto GC surfaces, containing about 20 μg of Pt, and left to dry at room temperature. After, **TeNTs/PtNPs/GC** electrodes were cycled by CV in phosphate buffer (pH 7.0, I = 0.2) starting from measured open circuit potential (OCP), between –400 mV and +800 mV at scan rate of 20 mV s^{-1}, until the current reached the steady-state conditions (typically 30 voltammetric cycles are required). The as obtained modified electrodes were washed after this electrochemical treatment and transferred in H_2SO_4 0.5 M electrolyte to be activated before their use as anodes and cathodes in phosphate buffer (pH 7.0, I = 0.2) solution for electrocatalytic methanol oxidation and O_2 reduction experiments, respectively.

4. Conclusions

The results of this work show the effectiveness of **TeNTs/PtNPs** nanostructures for methanol electrocatalytic oxidation (MOR) and oxygen reduction (ORR), at neutral conditions suitable for fuel cell applications. The full morphological and spectroscopic characterization of **TeNTs/PtNPs** synthesized structures was obtained by XRD, TEM, SAD and XPS techniques. Results confirm the formation of bulk structures constituted of Te nanotubes decorated with Pt nanoparticles, with a surface enriched in average with Pt and Te oxidized species compared to platinum and tellurium bulk composition. The presence of a Pt-Te interacting species phase, confirmed by XPS, represents the sites of Pt nucleation and growth directly grafted on Te nanotubes surface. The electrochemical characterization of **TeNTs/PtNPs** material in aqueous electrolytic solutions at pH 7.0 was tested by cyclic voltammetry experiments. The electrocatalytic activity enhancement of **TeNTs/PtNPs** structures for methanol oxidation and oxygen reduction, was proved by comparing the results with bare glassy carbon and bare platinum electrodes, as well as with the recent data reported in the literature on systems based on both platinum and platinum-free nanostructured materials. The experiments evidence that **TeNT/PtNP**, opportunely activated in sulphuric acid 0.5 M solution, is a promising versatile anode/cathode electrocatalyst material for (bio)- fuel cells applications, thus representing a valid alternative to pure platinum and platinum alloys based electrodes, that can operate with particular efficiency in safe neutral pH environment.

Supplementary Materials: The following are available online at www.mdpi.com/xxx/s1, Figure S1: Cyclic voltammetric curves on bare GC, bare Pt and **TeNT/PtNP/GC** electrodes at different methanol concentrations, after subtraction of the signal in absence of methanol. Figure S2: Cyclic voltammetric curves on bare GC, bare Pt and **TeNT/PtNP/GC** electrodes at O_2 atmospheric solution and O_2 saturated solutions after subtraction of the signal in absence of O_2.

Author Contributions: conceptualization, M.R.G. and A.T; methodology, F.M., M.R.G. and D.C.; data curation, E.F.; writing—original draft preparation, F.M. and M.R.G. writing—review and editing, M.R.G and A.T.

Funding: This research received no external funding.

Conflicts of Interest: The authors declare no conflict of interest.

References

1. Rao, C.N.R.; Kulkarni, G.U.; Thomas, P.J.; Edwards, P.P. Size-dependent chemistry: Properties of nanocrystals. *Chemistry – A European Journal* **2002**, *8*, 28-35.
2. Patzke, G.R.; Krumeich, F.; Nesper, R. Oxidic nanotubes and nanorods - anisotropic modules for a future nanotechnology. *Angew Chem Int Edit* **2002**, *41*, 2446-2461.
3. Iijima, S. Helical microtubules of graphitic carbon. *Nature* **1991**, *354*, 56-58.

4. Luo, X.L.; Morrin, A.; Killard, A.J.; Smyth, M.R. Application of nanoparticles in electrochemical sensors and biosensors. *Electroanal* **2006**, *18*, 319-326.
5. Sakamoto, M.; Takamura, K. Catalytic-oxidation of biological components on platinum-electrodes modified by adsorbed metals - anodic-oxidation of glucose. *Bioelectroch Bioener* **1982**, *9*, 571-582.
6. Chen, X.L.; Pan, H.B.; Liu, H.F.; Du, M. Nonenzymatic glucose sensor based on flower-shaped au@pd core-shell nanoparticles-ionic liquids composite film modified glassy carbon electrodes. *Electrochim Acta* **2010**, *56*, 636-643.
7. Toshima, N.; Yonezawa, T. Bimetallic nanoparticles - novel materials for chemical and physical applications. *New J Chem* **1998**, *22*, 1179-1201.
8. Liu, J.H.; Wang, A.Q.; Chi, Y.S.; Lin, H.P.; Mou, C.Y. Synergistic effect in an au-ag alloy nanocatalyst: Co oxidation. *J Phys Chem B* **2005**, *109*, 40-43.
9. Kim, M.J.; Lee, K.Y.; Jeong, G.H.; Jang, J.K.; Han, S.W. Fabrication of au-ag alloy nanoprisms with enhanced catalytic activity. *Chem Lett* **2007**, *36*, 1350-1351.
10. Booth, M.A.; Leveneur, J.; Costa, A.S.; Kennedy, J.; Travas-Sejdic, J. Tailoring the conductivity of polypyrrole films using low-energy platinum ion implantation. *J Phys Chem C* **2012**, *116*, 8236-8242.
11. Jin, G.P.; Li, J.; Peng, X. Preparation of platinum nanoparticles on polyaniline-coat multi-walled carbon nanotubes for adsorptive stripping voltammetric determination of formaldehyde in aqueous solution. *J Appl Electrochem* **2009**, *39*, 1889-1895.
12. Shi, L.; Liang, R.P.; Qiu, J.D. Controllable deposition of platinum nanoparticles on polyaniline-functionalized carbon nanotubes. *J Mater Chem* **2012**, *22*, 17196-17203.
13. Xia, B.Y.; Wu, H.B.; Wang, X.; Lou, X.W. One-pot synthesis of cubic ptcu3 nanocages with enhanced electrocatalytic activity for the methanol oxidation reaction. *J Am Chem Soc* **2012**, *134*, 13934-13937.
14. Xin, Y.C.; Liu, J.G.; Zhou, Y.; Liu, W.M.; Gao, J.A.; Xie, Y.; Yin, Y.; Zou, Z.G. Preparation and characterization of pt supported on graphene with enhanced electrocatalytic activity in fuel cell. *J Power Sources* **2011**, *196*, 1012-1018.
15. Singh, R.N.; Awasthi, R.; Sharma, C.S. Review: An overview of recent development of platinum-based cathode materials for direct methanol fuel cells. *Int J Electrochem Sc* **2014**, *9*, 5607-5639.
16. Yang, L.; Ge, J.J.; Liu, C.P.; Wang, G.L.; Xing, W. Approaches to improve the performance of anode methanol oxidation reaction-a short review. *Curr Opin Electrochem* **2017**, *4*, 83-88.
17. Jeon, T.Y.; Lee, K.S.; Yoo, S.J.; Cho, Y.H.; Kang, S.H.; Sung, Y.E. Effect of surface segregation on the methanol oxidation reaction in carbon-supported pt-ru alloy nanoparticles. *Langmuir* **2010**, *26*, 9123-9129.
18. He, C.; Desai, S.; Brown, G.; Bollepalli, S. In *Pem fuel cell catalysts: Cost, performance, and durability.* , The Electrochemical Society Interface, Fall 2005; pp 41-44.
19. Yue-Min, D.; Yao-Long, L.I.U.; Gui-Shi, R.A.O.; Guo-Fu, W.; Qi-Ling, Z.; Bin, R.E.N.; Zhong-Qun, T. Electrooxidation mechanism of methanol at pt-ru catalyst modified gc electrode in electrolytes with different ph using electrochemical and sers techniques. *Chinese J Chem* **2007**, *25*, 1617-1621.
20. Yan, B.; Concannon, N.M.; Milshtein, J.D.; Brushett, F.R.; Surendranath, Y. A membrane-free neutral ph formate fuel cell enabled by a selective nickel sulfide oxygen reduction catalyst. *Angew Chem Int Edit* **2017**, *56*, 7496-7499.
21. Tominaka, S.; Nishizeko, H.; Ohta, S.; Osaka, T. On-chip fuel cells for safe and high-power operation: Investigation of alcohol fuel solutions. *Energ Environ Sci* **2009**, *2*, 849-852.
22. Lehmann, K.; Yurchenko, O.; Urban, G. Carbon nanowalls for oxygen reduction reaction in bio fuel cells. *J. Phys.: Conf. Ser.* **2014**, *557*, 012008.

23. Santoro, C.; Arbizzani, C.; Erable, B.; Ieropoulos, I. Microbial fuel cells: From fundamentals to applications. A review. *J Power Sources* **2017**, *356*, 225-244.
24. Huang, M.H.; Wang, F.; Li, L.R.; Guo, Y.L. A novel binary pt3tex/c nanocatalyst for ethanol electro-oxidation. *J Power Sources* **2008**, *178*, 48-52.
25. Guascito, M.R.; Chirizzi, D.; Malitesta, C.; Siciliano, M.; Siciliano, T.; Tepore, A. Amperometric non-enzymatic bimetallic glucose sensor based on platinum tellurium microtubes modified electrode. *Electrochem Commun* **2012**, *22*, 45-48.
26. Guascito, M.R.; Chirizzi, D.; Malitesta, C.; Siciliano, T.; Tepore, A. Te oxide nanowires as advanced materials for amperometric nonenzymatic hydrogen peroxide sensing. *Talanta* **2013**, *115*, 863-869.
27. Siciliano, T.; Filippo, E.; Genga, A.; Micocci, G.; Siciliano, M.; Tepore, A. Single-crystalline te microtubes: Synthesis and no(2) gas sensor application. *Sensor Actuat B-Chem* **2009**, *142*, 185-190.
28. Guascito, M.R.; Chirizzi, D.; Malitesta, C.; Mazzotta, E.; Siciliano, M.; Siciliano, T.; Tepore, A.; Turco, A. Low-potential sensitive h2o2 detection based on composite micro tubular te adsorbed on platinum electrode. *Biosens Bioelectron* **2011**, *26*, 3562-3569.
29. Nist x-ray photoelectron spectroscopy database. https://srdata.nist.gov/xps/Default.aspx
30. Mayers, B.; Jiang, X.C.; Sunderland, D.; Cattle, B.; Xia, Y.N. Hollow nanostructures of platinum with controllable dimensions can be synthesized by templating against selenium nanowires and colloids. *J Am Chem Soc* **2003**, *125*, 13364-13365.
31. Bard, A.J.; Faulkner, L.R. *Electrochemical methods: Fundamentals and applications*. 2nd edition ed.; Wiley: 2000.
32. Chen, X.M.; Tian, X.T.; Zhao, L.M.; Huang, Z.Y.; Oyama, M. Nonenzymatic sensing of glucose at neutral ph values using a glassy carbon electrode modified with graphene nanosheets and pt-pd bimetallic nanocubes. *Microchim Acta* **2014**, *181*, 783-789.
33. Ernst, S.; Heitbaum, J.; Hamann, C.H. The electrooxidation of glucose in phosphate buffer solutions: Part i. Reactivity and kinetics below 350 mv/rhe. *J Electroanal Chem Interfacial Electrochem* **1979**, *100*, 173-183.
34. Park, S.; Boo, H.; Chung, T.D. Electrochemical non-enzymatic glucose sensors. *Anal Chim Acta* **2006**, *556*, 46-57.
35. Kadirgan, F.; Beden, B.; Leger, J.M.; Lamy, C. Synergistic effect in the electrocatalytic oxidation of methanol on platinum+palladium alloy electrodes. *J Electroanal Chem Interfacial Electrochem* **1981**, *125*, 89-103.
36. Filippo, E.; Baldassarre, F.; Tepore, M.; Guascito, M.R.; Chirizzi, D.; Tepore, A. Characterization of hierarchical alpha-moo3 plates toward resistive heating synthesis: Electrochemical activity of alpha-moo3/pt modified electrode toward methanol oxidation at neutral ph. *Nanotechnology* **2017**, *28*, 215601.
37. Rosenbaum, M.; Schroder, U.; Scholz, F. Investigation of the electrocatalytic oxidation of formate and ethanol at platinum black under microbial fuel cell conditions. *J Solid State Electr* **2006**, *10*, 872-878.
38. Sadhukhan, M.; Kundu, M.K.; Bhowmik, T.; Barman, S. Highly dispersed platinum nanoparticles on graphitic carbon nitride: A highly active and durable electrocatalyst for oxidation of methanol, formic acid and formaldehyde. *Int J Hydrogen Energ* **2017**, *42*, 9371-9383.
39. Jing, S.C.; Guo, X.L.; Tan, Y.W. Branched pd and pd-based trimetallic nanocrystals with highly open structures for methanol electrooxidation. *J Mater Chem A* **2016**, *4*, 7950-7961.
40. Li, H.H.; Zhao, S.; Gong, M.; Cui, C.H.; He, D.; Liang, H.W.; Wu, L.; Yu, S.H. Ultrathin ptpdte nanowires as superior catalysts for methanol electrooxidation. *Angew Chem Int Edit* **2013**, *52*, 7472-7476.
41. Xu, J.; Wang, Z.H.; Li, H.H.; Liu, J.W.; Yu, S.H. Templating synthesis of ternary ptpdte nanowires with tunable diameter for methanol electrooxidation. *Crystengcomm* **2016**, *18*, 4038-4041.
42. Nguyen, M.T.; Mecheri, B.; Iannaci, A.; D'Epifanio, A.; Licoccia, S. Iron/polyindole-based electrocatalysts to enhance oxygen reduction in microbial fuel cells. *Electrochim Acta* **2016**, *190*, 388-395.

43. Jin, Y.D.; Shen, Y.; Dong, S.J. Electrochemical design of ultrathin platinum-coated gold nanoparticle monolayer films as a novel nanostructured electrocatalyst for oxygen reduction. *J Phys Chem B* **2004**, *108*, 8142-8147.
44. Zhong, H.X.; Zhang, H.M.; Liang, Y.M.; Zhang, J.L.; Wang, M.R.; Wang, X.L. A novel non-noble electrocatalyst for oxygen reduction in proton exchange membrane fuel cells. *J Power Sources* **2007**, *164*, 572-577.
45. Salvi, A.M.; Pucciariello, R.; Guascito, M.R.; Villani, V.; Intermite, L. Characterization of the interface in rubber/silica composite materials. *Surf Interface Anal* **2002**, *33*, 850-861.